Numerical pump-probe experiments of laser-excited silicon in nonequilibrium phase

S. A. Sato,[1] K. Yabana,[2,1] Y. Shinohara,[1,3] T. Otobe,[4] and G. F. Bertsch[5]
[1]*Graduate School of Pure and Applied Sciences, University of Tsukuba, Tsukuba 305-8571, Japan*
[2]*Center for Computational Sciences, University of Tsukuba, Tsukuba 305-8577, Japan*
[3]*Max-Planck-Institute für Mikrostrukturphysik, Weinberg 2, D-06112 Halle, Germany*
[4]*Kansai Photon Science Institute, JAEA, Kizugawa, Kyoto 619-0615, Japan*
[5]*Department of Physics and Institute for Nuclear Theory, University of Washington, Seattle, Washington 98195, USA*
(Received 21 March 2013; revised manuscript received 26 January 2014; published 10 February 2014)

We calculate the dielectric response of crystalline silicon following irradiation by a high-intensity laser pulse, modeling the dynamics by the time-dependent Kohn-Sham equations in the presence of the laser field. Pump-probe measurements of the response are numerically simulated by including both pump and probe externals fields in the simulation. As expected, the excited silicon shows features of an electron-hole plasma of nonequilibrium phase in its response, characterized by a negative divergence in the real part of the dielectric function at small frequencies. The response to the probe pulse depends on the polarization of the pump pulse. We also find that the imaginary part of the dielectric function can be negative, particularly for the parallel polarization of pump and probe fields. We compare the calculated response with a simple Drude model. The real part of the dielectric function is well fitted by the model, treating the effective mass as a fitting parameter while taking electron density from the calculation. The fitted effective masses are consistent with carrier-band dispersions.

DOI: 10.1103/PhysRevB.89.064304 PACS number(s): 78.40.−q, 42.65.Re, 71.15.Mb, 77.22.−d

I. INTRODUCTION

The interaction of high-intensity and ultrashort electromagnetic fields with condensed matter is an important subject from both fundamental and technological points of view [1–5]. To investigate the dynamics of electrons and phonons in real time, the pump-probe experimental technique has been extensively employed. One example of its use is creating coherent phonons and measuring their properties [6]. The vibration is detected by measuring the change of reflectance of the probe pulse. However, this requires a good understanding of the dielectric properties of the surface excited by the pump pulse. Another example is the energy deposited by strong laser pulses close to the damage threshold. They produce high-density electron-hole pairs at the surface of dielectrics, causing strong reflection for the probe pulse [7]. It is even now possible to measure the population of high-density electron-hole pairs in the time resolution of less than a femtosecond [8–10]. However, the existing theory describing these effects is largely phenomenological. The dielectric properties of laser-excited material are often modeled with the Drude model [11–14], assuming that excited electrons behave like free carriers.

We have been developing a first-principles theoretical approach to describe electron dynamics in crystalline solids induced by the intense and ultrashort laser pulses. Time-dependent density functional theory (TDDFT) [15], treated in the adiabatic approximation, is a good candidate for a computational theory of the dynamics under those conditions. We have found it practical to solve the time-dependent Kohn-Sham (TDKS) equations in real space and real time [16], and have used this approach to model the optical breakdown of solids [17,18], coherent phonon generation [19,20], high harmonic generation [21], and coupled dynamics of electrons and electromagnetic fields in a multiscale description [22].

In the present paper, we apply the time-dependent Kohn-Sham equations to dielectric properties of a medium excited by short, intense laser pulses. However, in the interest of having a fully realistic simulation, we will deviate from our previous methodology by utilizing single-electron potentials that are better able to describe the electron structure of solids than the commonly used DFT functionals. Our method is to solve the TDKS equation in the medium in the presence of an external electromagnetic field having both pump and probe pulses. Thus, we simulate the pump-probe experiments numerically. The theory describes the electron dynamics fully quantum mechanically, but assumes that the electrons only interact via a time-dependent mean field. Thus, the theory is only expected to be justified before the times when electron-electron collisions have substantially affected the electronic structure. A separate issue is the creation of phonons. For the excitation energies we consider here, the electron-electron collision time sets a more stringent limit than the phonon interactions. To interpret the results, we compare with a simple Drude response of the excited quasiparticles, which are embedded in a dielectric medium [13,14].

At the next time scale, the electron-hole excitations will come to a kinetic equilibrium, so the system can be described as a thermalized electron-hole plasma with fixed numbers of electrons and holes. The dielectric properties of the equilibrated states are the subject of the companion paper [23]. At even later times, the ionic degrees of freedom will become thermalized as well. That complete plasma equilibrium is beyond the scope of the present work.

The construction of the paper is as follows. In Sec. II, we describe a method of numerical pump-probe simulation to extract dielectric properties of excited silicon. In Sec. III, we present results of the numerical pump-probe simulation for bulk silicon and compare them with a simple Drude model. Our findings are summarized in Sec. IV.

II. NUMERICAL PUMP-PROBE EXPERIMENTS

In this section, we carry out what we call numerical pump-probe experiments to study the dielectric properties

of the highly excited material in the nonequilibrium phase immediately after the irradiation of the laser pulse. We examine the electronic response in a unit cell of a crystalline solid irradiated by the pump and probe laser pulses. Since the wavelength of the laser pulses is much longer than a typical length scale of electron dynamics, we treat the laser electric field as a spatially uniform field, which is expressed using the vector potential $\vec{E}(t) = -\frac{1}{c}\frac{\partial}{\partial t}\vec{A}(t)$. The current induced by the probe pulse will be used to investigate the dielectric properties of excited matter. We note that the response formalism using a spatially uniform electric field has been developed to calculate the dielectric functions of solids [24–26].

A. Calculation of electron dynamics

Our calculation method has been described in detail elsewhere [19,22,24,27,28], so we only provide the details related to our study here. The electron dynamics is calculated using the TDKS equation,

$$i\hbar\frac{\partial}{\partial t}\psi_i(\vec{r},t) = h_{KS}(t)\psi_i(\vec{r},t), \tag{1}$$

where $h_{KS}(t)$ is a time-dependent Kohn-Sham Hamiltonian. It includes both scalar and vector potentials. The scalar potential has a lattice periodicity, including electron-ion and electron-electron interactions. The vector potential $\vec{A}(t)$ takes account of a spatially uniform electric field of the applied laser pulse. The vector potential $\vec{A}(t)$ appears in the kinetic term, $p^2/2m \to [\vec{p} + e\vec{A}(t)/c]^2/2m$. There is also a coupling to $\vec{A}(t)$ in the nonlocal part of the pseudopotential for the ions; see Refs. [24,27] for details. We calculate the dynamics of valence electrons only, treating the electron-ion interaction by the norm-conserving pseudopotential [29,30]. For the electron-electron interaction of the TDKS Hamiltonian, we employ the meta-generalized-gradient approximation (GGA) potential of Tran and Blaha [31] in the adiabatic approximation. This potential is not derived from an energy functional, but it allows the band gap to be properly treated [32]. Since we investigate a system in which a relatively small fraction of valence electrons is excited, it is important to use a functional which reproduces the band gap in the ground state. We have chosen the parameter c in the potential as $c = 1.04$ to reproduce the measured indirect band gap of silicon at 1.17 eV. We note that attempts to find functionals which provide better descriptions for optical properties are now under rapid progress [33–35]. We also note that, in the time-dependent current density functional theory, the exchange-correlation effect appears in the vector potential as well [36,37]. We simply ignore such effects in the present work.

The current flowing within the unit cell is given by

$$\vec{J}(t) = \sum_i \frac{1}{\Omega}\mathrm{Re}\left[\int_\Omega d\vec{r}\,\psi_i^*(\vec{r},t)\vec{j}(t)\psi_i(\vec{r},t)\right], \tag{2}$$

where Ω is the volume of the unit cell and the current operator $\vec{j}(t)$ is defined by

$$\vec{j}(t) = -\frac{e}{m}\frac{1}{i\hbar}[\vec{r},h_{KS}(t)]. \tag{3}$$

The relation of the vector potential $\vec{A}(t)$ in the unit cell to the external electromagnetic field exciting the system depends on a number of factors, including possible macroscopic polarization fields. A full description of the issue is presented in Ref. [22] where a coupled dynamics of macroscopic electromagnetic fields and microscopic electron dynamics is considered. In the present analysis, we use a transverse geometry [22] for the macroscopic shape where the sample is treated as infinite in the direction of the polarization vector so that there appears no polarization field inside the solid. Of course, the field is also affected by the absorption and the reflection from the surface region, but we do not attempt here to express the results in terms of the incident laser intensity. We take the following form for the vector potential of the pump pulse in the medium $A_P(t)$:

$$A_P(t) = \begin{cases} -c\frac{E_0}{\omega_P}\cos(\omega_P t)\sin^2(\pi t/\tau_L) & (0 < t < \tau_L) \\ 0 & (\text{otherwise}), \end{cases} \tag{4}$$

where ω_P and τ_L is the average frequency and the time length of the laser pulse, respectively. E_0 is the maximum electric-field strength in the medium. This is related to the maximum intensity of the pulse I by $I_v = cE_0^2/8\pi$ in the vacuum and $I_m = \epsilon^{1/2}cE_0^2/8\pi$ in the medium. Since the dielectric function ϵ is not well defined in the presence of a strong electric field, we shall report our results using the field intensity corresponding to the vacuum relationship.

Our computer code to solve the TDKS equation uses a three-dimensional grid representation to represent orbital wave functions. The unit cell for the silicon crystal treated has a length $a = 10.26$ a.u. and contains eight Si atoms. The cubic unit cell is discretized into 16^3 grid points. The four valence electrons of Si atoms beyond the closed $(1s2s1p)$ shells are treated dynamically. The k space is also discretized into 24^3 grid points. The time evolution is computed using a fourth-order Taylor expansion of the operator $\exp[-ih_{KS}(t)\Delta t/\hbar]$ [16]. We use a time step of $\Delta t = 0.08$ a.u. The number of time step is typically 24 000.

In Fig. 1, we show an example of the calculated electron dynamics induced by the intense pump pulse. Here the frequency of the pump pulse is set to $\hbar\omega_P = 1.55$ eV and the duration of the pump pulse is $\tau_L = 18$ fs. These values will be used in all calculations of this paper. For this figure, the maximum electric-field strength E_0 corresponds to an intensity of $I = 1.0 \times 10^{12}$ W/cm^2.

Figure 1(a) shows the time profile of the electric field, $E_P(t) = -\frac{1}{c}\frac{\partial}{\partial t}A_P(t)$. Figure 1(b) shows the induced current, calculated using the time-dependent orbitals in Eq. (2). The average frequency $\hbar\omega = 1.55$ eV is smaller than the direct band-gap energy (3.1 eV in the present calculation), so the initial current response is nondissipative since the field is sufficiently small. This is seen by the phase difference between the current and the electric field, which is shifted by $\pi/2$ at the beginning of the field pulse ($t < 5$ fs). As the intensity of the pulse increases, the system absorbs energy by the excitation of electron-hole pairs in the multiphoton absorption processes. As a result, the phase difference decreases. We also find a mixture of high-frequency component in the current after the maximum of the electric field. Making a Fourier analysis, we find that it is dominated by frequencies around 4.2 eV/$\hbar$, slightly higher than the frequency of the optical band gap of 3.2 eV in the present calculation.

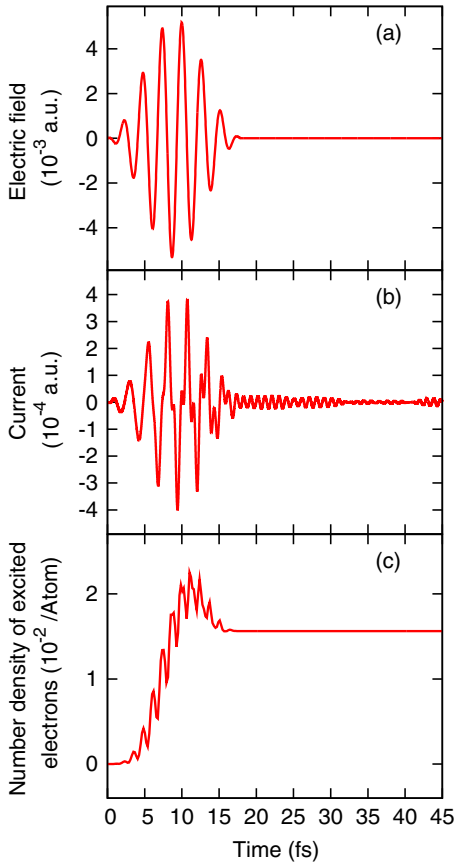

FIG. 1. (Color online) (a) The time profile of the electric field applied to crystalline silicon. The laser intensity corresponds to $I = 1.0 \times 10^{12}$ W/cm^2. (b) The current induced by the applied electric field. (c) The number density of excited electrons per atom.

Figure 1(c) shows the number density of excited electron-hole pairs per Si atom. To calculate it, we first define eigenstates of the Kohn-Sham Hamiltonian of the excited system. We consider a system at a time t and denote the Kohn-Sham Hamiltonian of Eq. (1) at the time t as $h_{KS}(t)$. We introduce the Kohn-Sham orbitals which satisfy the following eigenvalue equations:

$$\hat{h}_{KS}(t)\phi_i^t = \epsilon_i^t \phi_i^t. \tag{5}$$

Note that the Kohn-Sham Hamiltonian $\hat{h}_{KS}(t)$ is different from that of the initial state due to the change in electron density in the excited system as well as an addition of the electric field of applied laser pulse. Using eigenfunctions ϕ_i^t, we may define the number density of electron-hole pairs by

$$n_{eh}(t) = \sum_i \left\{ 1 - \sum_j \left| \langle \phi_j^t | \psi_i(t) \rangle \right|^2 \right\}, \tag{6}$$

where the sum over i, j is taken over occupied orbitals, and $|\psi_i(t)\rangle$ is the orbital of the TDKS equation at time t. From Fig. 1(c), we find a rapid increase of the excited electrons during the field pulse. After the pulse ends, the number density is independent of time, showing that the present adiabatic framework does not include any recombination mechanisms.

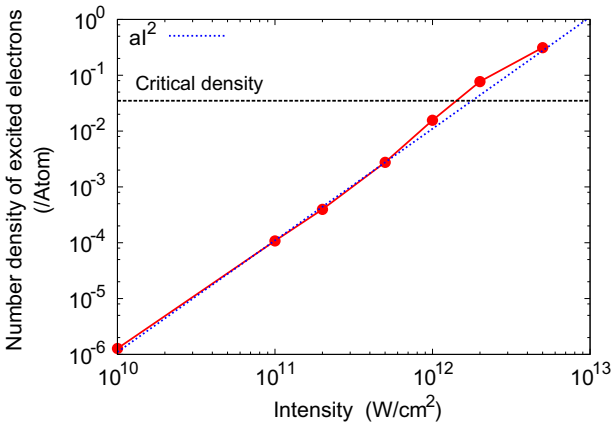

FIG. 2. (Color online) The number density of electron-hole pairs of the crystalline silicon in the final state following the pulsed excitation as a function of the maximum pump intensity determined as $I = cE_0^2/8\pi$. The critical density is indicated by the horizontal line. The squared intensity line normalized at 10^{10} W/cm^2 is also shown by the blue dotted line.

We next discuss the number density of excited electron-hole pairs after the laser pulse ends for different intensities. Figure 2 shows the result. As seen from the figure, the number of excited electrons increases with increasing the applied field intensity. At a low-intensity region, they scale with the square of the field intensity. This is because two photons are required for electrons to be excited across the direct band gap. In the figure, the horizontal line indicates the critical number density; the plasma frequency of this critical density coincides with the frequency of the incident laser pulse. At around the field intensity of 1.0×10^{12} W/cm^2 corresponding to the critical number density, the number density of electron-hole pairs becomes larger than the intensity squared line. As will be seen later, the dielectric property of excited matter shows a large change from that in the ground state at field intensities around this value and above.

B. Dielectric function from numerical pump-probe calculation

To extract dielectric properties of excited matter, we compare two calculations, one solving the TDKS equation of Eq. (1) with the vector potential containing pump and probe pulses and the other containing the pump pulse only. We denote the electric field of the pump pulse as $E_P(t)$ and that of the probe pulse as $E_p(t)$. We denote the current in the calculations containing the pump pulse only as $J_P(t)$ and that in the calculations containing both pump and probe pulses as $J_{Pp}(t)$. We define the current induced by the probe pulse as the difference,

$$J_p(t) = J_{Pp}(t) - J_P(t). \tag{7}$$

From the probe current $J_p(t)$, we may extract the electric conductivity $\sigma(\omega)$ and the dielectric function $\epsilon(\omega)$ of excited matter by the following equations:

$$\sigma(\omega) = \frac{\int dt\, J_p(t) e^{i\omega t}}{\int dt\, E_p(t) e^{i\omega t}}, \tag{8}$$

$$\epsilon(\omega) = 1 + \frac{4\pi i \sigma(\omega)}{\omega}. \tag{9}$$

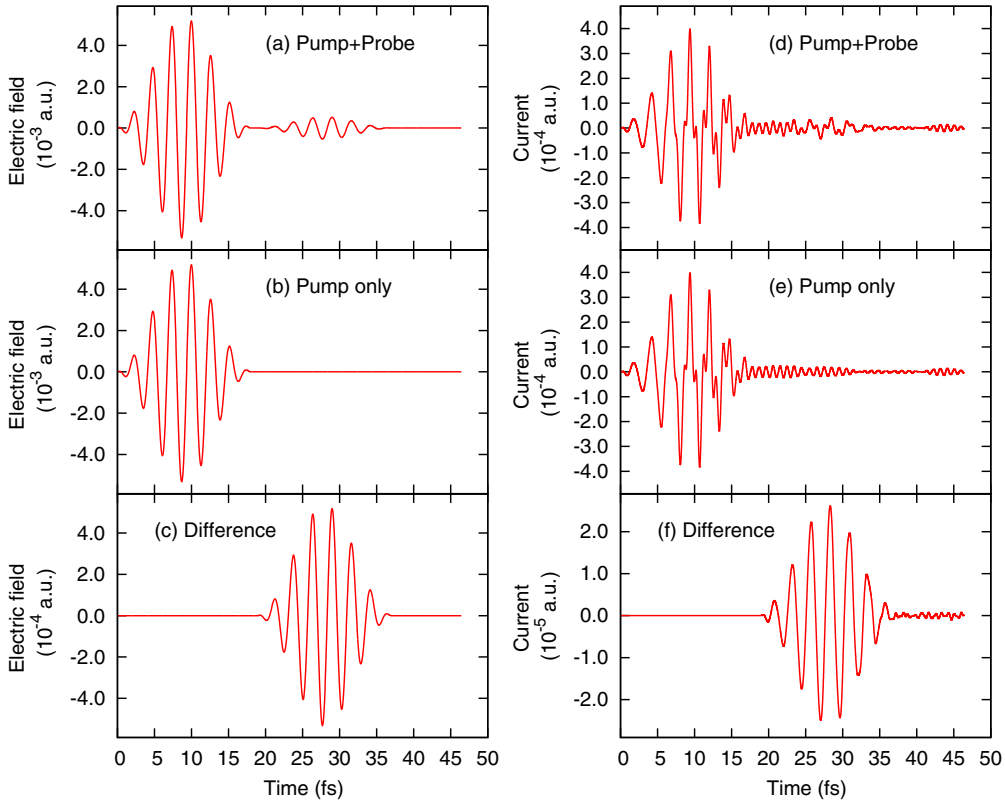

FIG. 3. (Color online) Left panels show the electric field of (a) pump and probe pulses, (b) pump pulse, and (c) probe pulse. Right panels show the current induced by the (d) pump plus probe pulse and (e) pump pulse only, and (f) the difference of the currents shown in (d) and (e).

We note that, in principle, the above-defined conductivity and dielectric function depend also on the time delay τ_{Pp} between the pump and probe pulses. We will later show that the dependence on delay time is rather small, at least for the real part of the dielectric function.

In practice, we employ the vector potential of the form of Eq. (4) as the pump pulse. As for the probe pulse, we use the same functional form as Eq. (4) delayed by an amount τ_{Pp} from the pump pulse,

$$A_p(t) = -c\frac{e_0}{\omega_p}\cos[\omega_p(t-\tau_{Pp})] \times \sin^2[\pi(t-\tau_{Pp})/\tau_L], \tag{10}$$

for $\tau_{Pp} < t < \tau_L + \tau_{Pp}$ and zero otherwise.

In Fig. 3, we show typical time profiles of the electric fields and the induced currents for a delay time of $\tau_{Pp} = 19$ fs. The pump pulse is the same as in Fig. 1, with a maximum intensity of 1.0×10^{12} W/cm^2. The probe intensity is a factor of 100 smaller, which we deem to be sufficiently weak to extract the linear response. In the left panels of Fig. 3, we show electric fields of (a) pump and probe pulses $E_P(t) + E_p(t)$, (b) pump pulse $E_P(t)$, and (c) probe pulse $E_p(t)$, as functions of the time. The right panels show currents induced by the (d) pump and probe pulses $J_{Pp}(t)$, (e) pump pulse only $J_P(t)$, and (f) the difference of the currents $J_p(t)$ of Eq. (7).

The next step is to calculate the dielectric function from the probe current using Eqs. (8) and (9). The pump-probe calculation using the probe pulse of Eq. (10) and the probe current of Eq. (7) gives us dielectric properties around the average frequency $\hbar\omega_p$. To explore the dielectric properties for a wide frequency region, we repeat the pump-probe calculations for different frequencies of the probe pulses.

In Fig. 4, we show typical calculations using a number of probe pulses of differing frequencies. Figures 4(a) and 4(b) show the absolute values of the Fourier transforms of $E_p(t)$ and $J_p(t)$, respectively. Figures 4(c) and 4(d) show the real and imaginary parts of the dielectric function, which is calculated using Eqs. (8) and (9). The curve is composed of a number of curves with different colors for each probe frequency. One can see that the overlap is very good for the different average probe frequencies, validating our method to extract the dielectric function.

We have carried out the pump-probe simulations for several intensities of the pump pulse. The results for the dielectric functions are shown in Fig. 5. The real and the imaginary parts are presented in Figs. 5(a) and 5(b), respectively.

The distinguishing feature in the response is the negative divergence at small frequencies seen in the real part. This arises from the quasiparticles in the excited system, as we will see more quantitatively later. The imaginary part of the response is not quite as simple to analyze. At the strongest case of $I = 5.0 \times 10^{12}$ W/cm^2, the dielectric functions calculated using probe pulses of different central frequencies are not connected smoothly. This indicates the imaginary part of the dielectric function is not well defined under strong excitation.

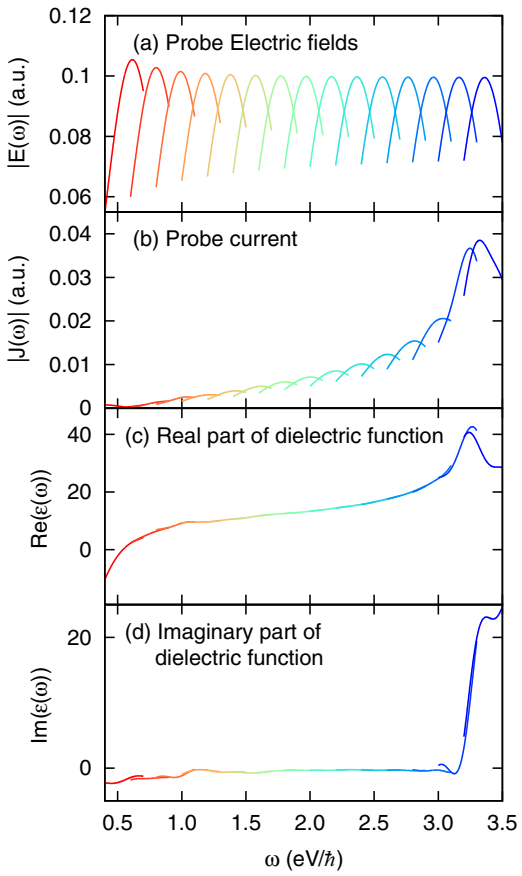

FIG. 4. (Color online) The top two panels show the Fourier transformations of the probe electric field $E_p(\omega)$ and the probe current $J_p(\omega)$. The bottom two panel shows the real and imaginary parts of the dielectric function extracted from $E_p(\omega)$ and $J_p(\omega)$ through Eqs. (8) and (9). The pump pulse has an intensity $I = 1.0 \times 10^{12}$ W/cm^2 and an average frequency $\omega_P = 1.55$ eV/$\hbar$. The polarization directions of the pump and probe pulses are taken to be parallel.

An interesting feature of the TDDFT response is that the dielectric tensor is not isotropic in the excited crystal, even though the crystal symmetry is cubic. This may be seen in Fig. 6, comparing the dielectric functions for the probe polarization either parallel or perpendicular to the pump polarization.

The real part of the dielectric function shows the low-frequency plasmon response more strongly for the parallel component. One may notice that Im[$\epsilon(\omega)$] is negative at some frequencies when pump and probe pulses are parallel. This was also observed in Fig. 4(d). This might indicate a population inversion that could sustain a growth of intensity at those frequencies. However, one should carry the full calculation of the pulse propagating in space as well as time [22] to assert that the excited medium can amply the pulses.

We next ask how sensitive the extracted dielectric function is to the time delay of the probe pulse. Since there are no dissipative processes in the adiabatic TDDFT, the properties of the system should not change after some initial period when the phases of the excited orbitals become incoherent. Figure 7 shows how the extracted dielectric function depends on delay time for the case of strongest laser intensity shown in Fig. 5.

We have selected delay times over a range that corresponds to a full cycle of the pump pulse, since that frequency could be imprinted on the phases of the particle at later times. The range of the delay times is 19.00, 19.67, 20.33, and 21.67 fs. The latter three delay times correspond to a quarter, a half, and one period of the pump pulse $2\pi/\omega_P$ added to the first time. One can see that the variation of the real part is rather small, considering that the dielectric function without laser distortion is in the range of 10–15. The imaginary part, however, shows different behavior. Although the average values over the frequency region are more or less similar, the frequency dependences show substantial variation. This fact indicates that the imaginary part of the dielectric function is not well defined after the irradiation of the strong pump pulse and is consistent with the observation in Fig. 5(b).

We found the same behavior for other cases of time delays as well. Namely, the real part is mostly independent of delay, even extending the delay to very large times. The imaginary part is only qualitatively similar for different delay times for strong pump cases. In the sequel, we will analyze all of the results using the dielectric function at $\tau_{Pp} = 19$ fs, and one

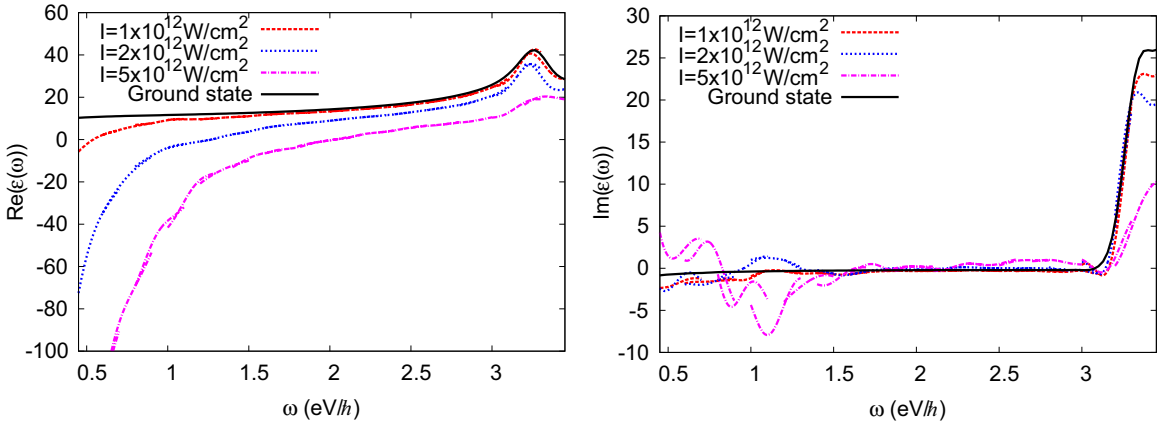

FIG. 5. (Color online) (a) Real and (b) imaginary parts of the dielectric functions of Si excited by field pulses of three intensities. The dielectric functions are deduced using pump-probe calculations. The polarization direction of the probe pulse is taken to be parallel to that of the pump pulse. The dielectric function of silicon in the ground state is also shown.

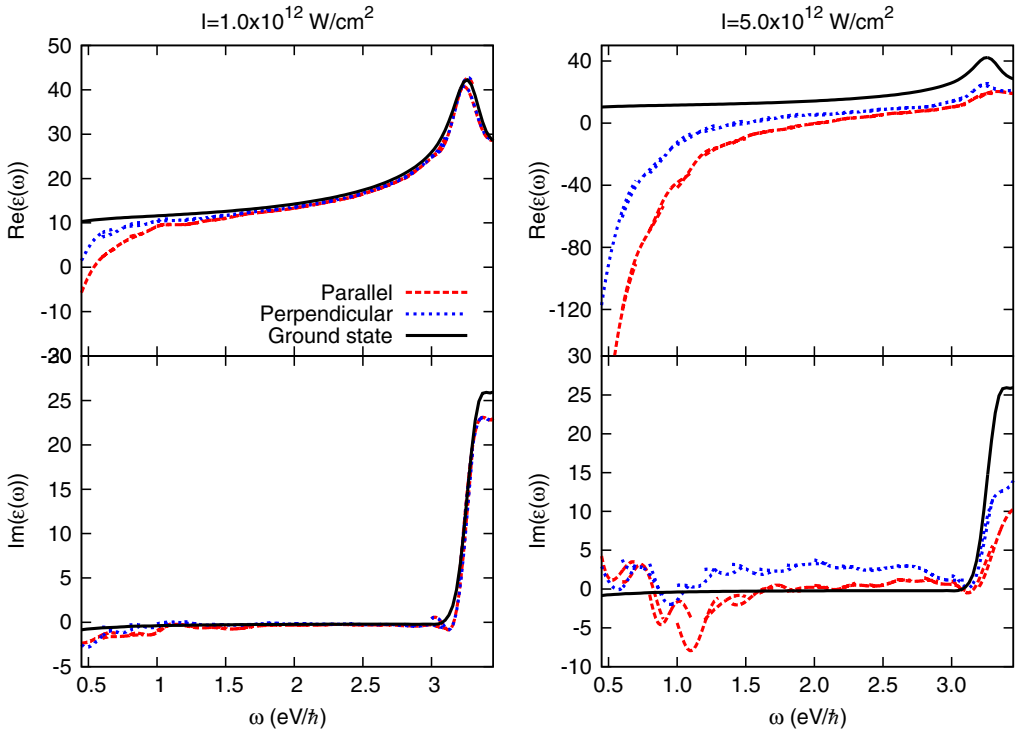

FIG. 6. (Color online) Comparison of dielectric functions of excited silicon probed with either parallel or perpendicular direction to the pump fields. Red dashed curves show results of parallel probe cases, blue dotted curves show results of perpendicular probe cases, and the black solid curves show dielectric function without the pump pulse.

should remember that the imaginary part is less well defined than the real part.

III. COMPARISON WITH FREE-CARRIER MODELS

Dielectric properties of solids excited by intense and ultrashort laser pulses are often modeled employing a simplified dielectric function, adding a Drude-like component to the dielectric function in the ground state [13,14]. In this section, we will examine how well the dielectric function of excited matter in the present calculation may be described by a simplified dielectric model.

First we consider an embedded Drude model, the dielectric function given as a sum of the ground-state response and the Drude response of free carriers,

$$\epsilon_{ED}(\omega) = \epsilon_0(\omega) - 4\pi i \frac{e^2 n_{eh}}{m^* \omega(\omega + i/\tau)}. \tag{11}$$

Here, $\epsilon_0(\omega)$ is the dielectric function in the ground state, n_{eh} is the electron-hole density, m^* is the reduced mass of electron holes, and τ is the Drude damping time. For the dielectric function in the ground state, $\epsilon_0(\omega)$, we will use the values obtain from the present calculation. The number density of electron-hole pairs, n_{eh}, is extracted from the calculation using Eq. (6). We treat m^* and τ as parameters, fitting to the calculated $\epsilon(\omega)$.

Sokolowski-Tinten and von der Lind proposed a more sophisticated model for the dielectric function excited by

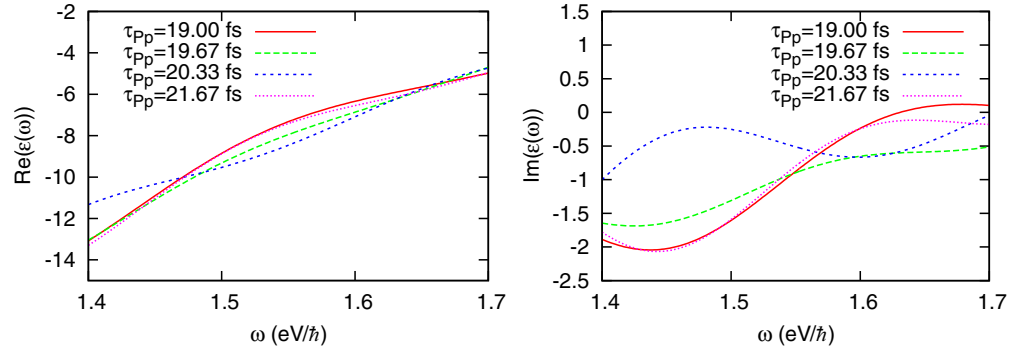

FIG. 7. (Color online) Extracted dielectric functions as a function of the delay time τ_{Pp}. The pump pulse has an intensity $I = 5.0 \times 10^{12}$ W/cm^2 and an average frequency $\omega_P = 1.55$ eV/$\hbar$. The probe frequency is $\omega_p = 1.55$ eV/$\hbar$ and its delay times for the four graphed lines are $\tau_{Pp} = 19{,}0$, 19.67, 20.33, and 21.67 fs. The polarization directions of the pump and probe pulses are taken to be parallel.

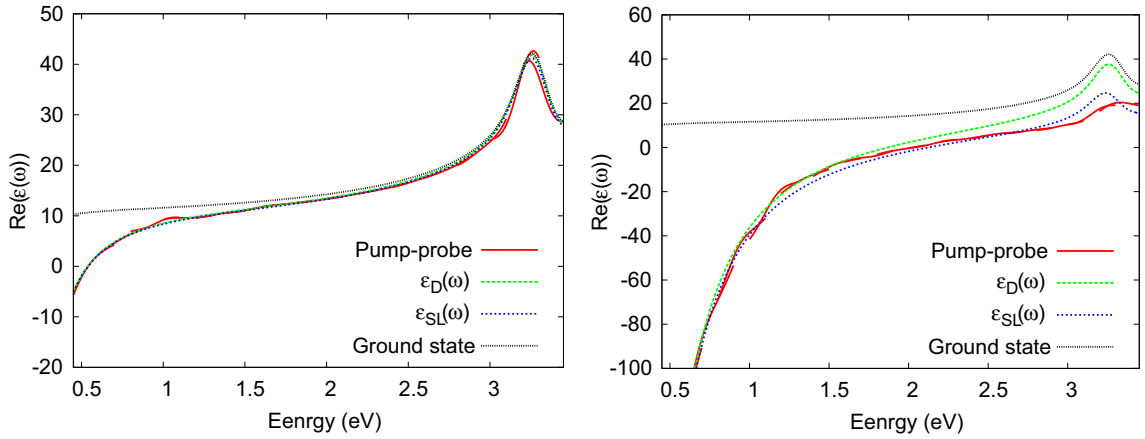

FIG. 8. (Color online) Dielectric function of silicon excited by two field pulses, 1.0×10^{12}W/cm^2 (left panels) and 5.0×10^{12}W/cm^2 (right panels), is fitted by the embedded Drude model and by the SL model. The polarization directions of the pump and probe pulse are taken to be parallel.

strong laser fields [7], which we shall call the SL model. They consider three physical effects for the dielectric response of a laser-excited semiconductor: (i) state and band filling, (ii) renormalization of the band structure, and (iii) the free-carrier response. The SL dielectric function is parameterized as

$$\epsilon_{SL}(\omega) = 1 + [\epsilon_0(\omega + \Delta E_{\rm gap}) - 1]\frac{n_0 - n_{eh}}{n_0} - 4\pi i \frac{e^2 n_{eh}}{m^*\omega(\omega + i/\tau)}, \quad (12)$$

where $\Delta E_{\rm gap}$ is the change of the band gap by the laser irradiation and n_0 is the density of electrons which contribute to the dielectric response. For $\Delta E_{\rm gap}$, we use a change of single-particle energies, $\epsilon_i^{t_f}$, of Eq. (5) at the time $t = t_f$ after the laser pulse ended. We treat the active number of valence electrons, n_0, as a fitting parameter.

We achieved the fits only to the real part of the dielectric function, which shows a smooth behavior as seen in Fig. 5. The imaginary part, which shows negative value for certain frequencies, cannot be described reasonably with the Drude model. Figure 8 shows the fits obtained in the embedded Drude model and the SL model for two intensities of the pump field. The polarization directions of the pump and probe pulses are taken to be parallel. The real part of the dielectric function is well fitted by both models. At higher intensity, both models describes well at lower frequencies, but the SL model fits better above the direct band gap.

In the fitting procedure, we found the effective mass is sensitive and can be determined without ambiguity. The effective mass for the pump pulse of 1.0×10^{12} W/cm^2 is given by $m^* = 0.35$, while the effective mass for the pump pulse of 5.0×10^{12} W/cm^2 is given by $m^* = 0.45$. The real part of the dielectric function is not sensitive to the collision time. In the fit, we use $\tau = 25$ fs, but other values give a similar curve. We have also achieved fits to the case of the probe pulse polarization perpendicular to the pump one. The effective mass for the pump pulse of 1.0×10^{12} W/cm^2 is given by $m^* = 0.70$, while the effective mass for the pump pulse of 5.0×10^{12} W/cm^2 is given by $m^* = 0.85$. We thus find that the effective mass increases as the pump intensity increases. The effective mass is also larger for the cases of perpendicular polarizations of pump and probe pulses than for the parallel case.

The effective mass and its change with the pump intensity and polarization may be understood from the band structure. A weak pump pulse excites electrons at specific k points by two-photon absorption, while a strong pump pulse excites electrons at various k points by tunnel and multiphoton excitations. The effective mass of electrons depends very much on the their positions in the bands.

In the SL fitting, we use a change of energy gap, ΔE_g, estimated from $\epsilon_i^{t_f}$. This is a small negative value, $\Delta E_g \simeq 0.01$ eV. The gap narrowing in highly excited matter has been an actively discussed issue, both experimentally and theoretically. A much larger amount of decrease than the present analysis has been theoretically reported and attributed to a change of dielectric screening effects [38,39]. This is an electron correlation effect which requires a treatment beyond the adiabatic TDDFT.

IV. SUMMARY

We proposed a computational methodology to investigate the effect of ultrashort laser pulses on the dielectric properties of bulk solids, mimicking the pump-probe experiments used to measure the effects. As we have shown, it is practical to carry out the simulation by solving the time-dependent Kohn-Sham equation in real time, including electric fields of both pump and probe pulses. The simulation makes it possible to investigate dielectric properties of excited matter in the nonequilibrium phase before any collision effects start to become significant.

We presented calculations for bulk silicon irradiating a pump pulse of 1.55 eV and probe pulses of various central frequencies and polarizations. The meta-GGA functional which reproduces the band gap is employed. We found that the real part of the dielectric function can be reliably extracted in the numerical pump-probe experiment. It shows a metallic response reflecting dense electron-hole pair excitations. The imaginary part of the dielectric function is less well defined,

especially at strong excitations. It has a negative value at certain frequencies, indicating a possible amplification of the laser pulse. The extracted dielectric function also shows anisotropy in the direction relative to the pump polarization direction. The difference comes from the nonequilibrium distributions of electrons and holes in k space.

A simple model can be constructed using ingredients of the Drude model of free-electron dynamics. The real part of the dielectric function was found to be well described by a Drude-like contribution of the excited quasiparticles embedded in the dielectric medium corresponding to the ground state. In the embedded Drude model, there are three parameters determining the quasiparticle plasmon contribution, namely, the density of quasiparticles, their effective mass m^*, and the collision time τ. The density of quasiparticles is known from the numerical simulation, but the other quantities are fit. From the real part of the dielectric function, we find that the effective mass increases with increasing pump field intensity, as expected from the band structure. We also find the effective mass depends on the relative direction between the pump and probe pulses, with a larger value in the perpendicular case than in the parallel case. The collision time cannot be determined reliably from the present numerical pump-probe calculation.

ACKNOWLEDGMENTS

This work is supported by the Grants-in-Aid for Scientific Research No. 23340113, No. 23104503, No. 21340073, and No. 21740303. The numerical calculations were performed on the supercomputer at the Institute of Solid State Physics, University of Tokyo, and T2K-Tsukuba at the Center for Computational Sciences, University of Tsukuba. G.F.B. acknowledges support by the National Science Foundation under Grant No. PHY-0835543 and by the US Department of Energy under Grant No. DE-FG02-00ER41132.

[1] M. D. Perry, B. C. Stuart, P. S. Banks, M. D. Feit, V. Yanovsky, and A. M. Rubenchik, J. Appl. Phys. **85**, 6803 (1999).
[2] T. Brabec and F. Krausz, Rev. Mod. Phys. **72**, 545 (2000).
[3] A. Couairon and A. Mysyrowicz, Phys. Rep. **441**, 47 (2007).
[4] E. G. Gamaly, Phys. Rep. **508**, 91 (2011).
[5] P. Balling and J. Schou, Rep. Prog. Phys. **76**, 036502 (2013).
[6] R. Merlin, Solid State Commun. **102**, 207 (1997).
[7] K. Sokolowski-Tinten and D. von der Linde, Phys. Rev. B **61**, 2643 (2000).
[8] M. Schultze, E. M. Bothschafter, A. Sommer, S. Holzner, W. Schweinberger, M. Fiess, M. Hofstetter, R. Kienberger, V. Apalkov, V. S. Yakovlev, M. I. Stockman, and F. Krausz, Nature (London) **493**, 75 (2013).
[9] A. Schiffrin, T. Paasch-Colberg, N. Karpowicz, V. Apalkov, D. Gerster, S. Mühlbrandt, M. Korbman, J. Reichert, M. Schultze, S. Holzner, J. Barth, R. Kienberger, R. Ernstorfer, V. Yakovlev, M. I. Stockman, and F. Krausz, Nature (London) **493**, 70 (2013).
[10] A. V. Mitrofanov, A. J. Verhoef, E. E. Serebryannikov, J. Lumeau, L. Glebov, A. M. Zheltikov, and A. Baltuska, Phys. Rev. Lett. **106**, 147401 (2011).
[11] A. Kaiser, B. Rethfeld, M. Vicanek, and G. Simon, Phys. Rev. B **61**, 11437 (2000).
[12] B. Rethfeld, Phys. Rev. Lett. **92**, 187401 (2004).
[13] N. Medvedev and B. Rethfeld, J. Appl. Phys. **108**, 103112 (2010).
[14] B. Rethfeld, O. Brenk, N. Medvedev, H. Krutsch, and D. H. H. Hoffmann, Appl. Phys. A **101**, 19 (2010).
[15] E. Runge and E. K. U. Gross, Phys. Rev. Lett. **52**, 997 (1984).
[16] K. Yabana and G. F. Bertsch, Phys. Rev. B **54**, 4484 (1996).
[17] T. Otobe, M. Yamagiwa, J.-I. Iwata, K. Yabana, T. Nakatsukasa, and G. F. Bertsch, Phys. Rev. B **77**, 165104 (2008).
[18] T. Otobe, K. Yabana, and J.-I. Iwata, J. Phys. Cond. Matter **21**, 064224 (2009).
[19] Y. Shinohara, K. Yabana, Y. Kawashita, J.-I. Iwata, T. Otobe, and G. F. Bertsch, Phys. Rev. B **82**, 155110 (2010).
[20] Y. Shinohara, S. A. Sato, K. Yabana, T. Otobe, J.-I. Iwata, and G. F. Bertsch, J. Chem. Phys. **137**, 22A527 (2012).
[21] T. Otobe, J. Appl. Phys. **111**, 093112 (2012).
[22] K. Yabana, T. Sugiyama, Y. Shinohara, T. Otobe, and G. F. Bertsch, Phys. Rev. B **85**, 045134 (2012).
[23] S. A. Sato, K. Yabana, Y. Shinohara, and T. Otobe (unpublished).
[24] G. F. Bertsch, J.-I. Iwata, A. Rubio, and K. Yabana, Phys. Rev. B **62**, 7998 (2000).
[25] F. Kootstra, P. L. de Boeij, and J. G. Snijders, Phys. Rev. B **62**, 7071 (2000).
[26] C. Attaccalite, M. Grüning, and A. Marini, Phys. Rev. B **84**, 245110 (2011).
[27] K. Yabana, T. Nakatsukasa, J.-I. Iwata, and G. F. Bertsch, Phys. Status Solidi (B) **243**, 1121 (2006).
[28] G. F. Bertsch and K. Yabana, in *Introduction to Computational Methods in Many Body Physics*, edited by M. Bonitz and D. Semkat (Rinton, Princeton, NJ, 2006), Chap. 3.
[29] N. Troullier and J. L. Martins, Phys. Rev. B **43**, 1993 (1991).
[30] L. Kleinman and D. M. Bylander, Phys. Rev. Lett. **48**, 1425 (1982).
[31] F. Tran and P. Blaha, Phys. Rev. Lett. **102**, 226401 (2009).
[32] D. Koller, F. Tran, and P. Blaha, Phys. Rev. B **85**, 155109 (2012).
[33] F. Sottile, V. Olevano, and L. Reining, Phys. Rev. Lett. **91**, 056402 (2003).
[34] V. U. Nazarov and G. Vignale, Phys. Rev. Lett. **107**, 216402 (2011).
[35] S. Sharma, J. K. Dewhurst, A. Sanna, and E. K. U. Gross, Phys. Rev. Lett. **107**, 186401 (2011).
[36] G. Vignale and W. Kohn, Phys. Rev. Lett. **77**, 2037 (1996).
[37] J. A. Berger, P. L. de Boeij, and R. van Leeuwen, Phys. Rev. B **75**, 035116 (2007).
[38] A. Oschlies, R. W. Godby, and R. J. Needs, Phys. Rev. B **45**, 13741 (1992).
[39] S. V. Faleev, M. van Schilfgaarde, T. Kotani, F. Léonard, and M. P. Desjarlais, Phys. Rev. B **74**, 033101 (2006).